Influence of the Semiconducting Properties of a Current Collector on the Electric Double Layer Formation on Porous Carbon

Jun-Nan Nian and Hsisheng Teng*

Department of Chemical Engineering and the Center for Micro/Nano Technology Research, National Cheng Kung University, Tainan 70101, Taiwan

Received: December 22, 2004; In Final Form: March 26, 2005

The electrochemical behavior of polyacrylonitrile-based activated carbon cloth combined with a stainless steel current collector was examined using ac impedance spectroscopy. H_2SO_4, KOH, and KNO_3 were employed as the electrolytes. The data presented in the impedance complex plane exhibit a semicircle at high frequencies followed by a vertical line at low frequencies. The high frequency data were found to be characteristic of the space charge region of the semiconducting oxide layer on the stainless steel, while the low frequency data depicted the double layer formation on the porous carbon. The double layer capacitance was found to decrease with the space charge resistance, which was potential dependent and a major contribution to the overall resistance of the carbon/stainless steel electrode. The electrolyte type affected the potential window employed in energy storage and thus the semiconducting behavior of the oxide layer. Both the n- and p-type semiconductors in depletion condition appeared within the potential window applied for the H_2SO_4 electrolyte, and this caused the presence of a peak capacitance. Only the n-type depletion condition was found in the KNO_3 and KOH electrolytes with the p-type oxide situated in accumulation at the potentials applied, and thus, the capacitance was larger at more negative potentials.

Introduction

Electrochemical capacitors (ECs) have been considered a possible substitute for rechargeable batteries employed in consumer electronic products and electric vehicles that require pulse-current supply.[1] This is attributed to the fact that ECs have an energy density comparable to that of batteries but a much higher power density. Porous carbon with a high surface area is the electrode material extensively used for ECs, due to the large electrode/electrolyte interface available for double layer formation to store energy.[2−13]

Stainless steel foil, which possesses an anticorrosion oxide layer, has been widely used as the current collector for carbon in ECs. However, little attention has been paid to the fact that the oxide layer usually behaves like a n- or p-type semiconductor, depending on the potential applied.[14,15] The performance of the carbon/stainless steel composite electrode must be influenced by the semiconducting properties of the foil.

There have been numerous studies on the analysis of the electrode interface behaviors using impedance spectroscopy techniques,[16−18] and the significant influence of the semiconducting properties of the current collector on the overall electrode performance has been pointed out.[18] The impedance data can be simulated with a suitable equivalent circuit to give electrochemical parameters of reasonable physical meanings.[19−21] The electrode system in ECs has been analyzed by the impedance method.[6,22] However, there are still sophisticated impedance behaviors observed and a detailed explanation for the observation is rarely given. For example, it has been encountered that a carbon/stainless steel composite electrode showed unexpected capacitive responses due to the change in the potential applied or the electrolyte employed.[6,22] This is an important issue that has to be resolved to optimize the performance of ECs.

In the present work, impedance measurements on porous carbon electrodes assembled with a stainless steel current collector are carried out in aqueous electrolyte solutions. How the intrinsic characteristics of stainless steel may have eventually affected the overall performance of the composite electrode, especially the capacitive response to the semiconducting oxide layer, will be extensively discussed. The aim of this work is to shed some light on the above-mentioned aspects, through appropriate interpretation of the obtained impedance results.

Experimental Section

Polyacrylonitrile (PAN)-based activated carbon cloth supplied by Taiwan Carbon Technology Co., Taiwan, served as the porous carbon electrode for electrochemical measurements in the present work. To avoid any intrusion of unexpected influence from retained carbon surface oxides, the carbon cloth was cleaned by treatment at 900 °C in helium for 20 min, prior to any further characterization or measurement. The BET surface area and pore volume of the carbon were determined, from N_2 adsorption, to be 960 $m^2\ g^{-1}$ and 0.46 $cm^3\ g^{-1}$, respectively. This carbon is mainly microporous, indicated by its N_2 isotherm of type I.

The electrochemical measurements were carried out in a three-electrode cell using Ag/AgCl and Pt as the reference and counter electrodes, respectively. The working electrode consisted of 2 cm^2 carbon cloth and stainless steel foil (type 304) as the current collector. The carbon cloth was attached to the stainless steel foil by a physical contact with pressure being applied. All electrochemical measurements were carried out at ambient

* To whom correspondence should be addressed. E-mail: hteng@mail.ncku.edu.tw. Phone: 886-6-2385371. Fax: 886-6-2344496.

10.1021/jp044171s CCC: $30.25
Published on Web 04/26/2005

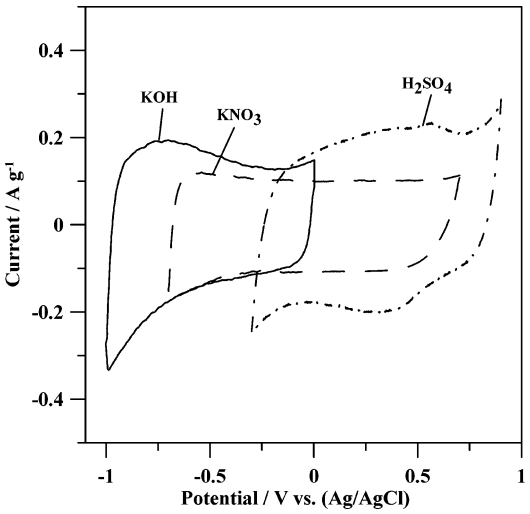

Figure 1. Cyclic voltammograms of the carbon/stainless steel electrode in 1.5 M KOH, 1.5 M KNO_3, and 0.5 M H_2SO_4 at a scan rate of 1 mV s^{-1}.

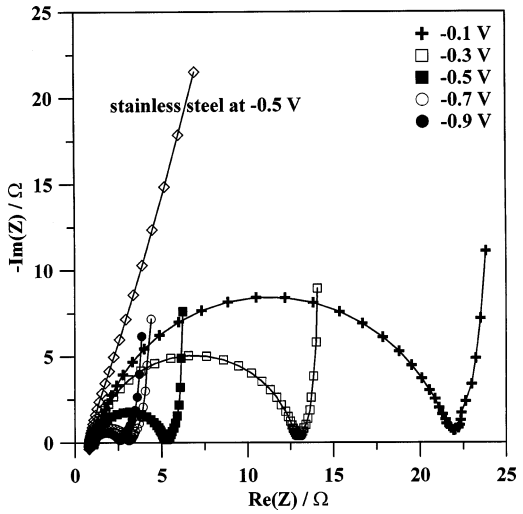

Figure 2. Nyquist impedance spectra of the carbon/stainless steel electrode obtained at different potentials in 1.5 M KOH. The spectrum of the stainless steel at −0.5 V is also given.

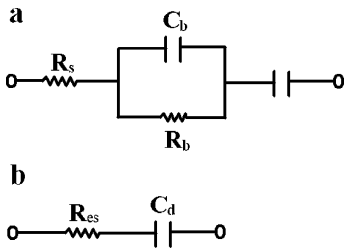

Figure 3. Equivalent circuits for the impedance spectra of the carbon/stainless steel electrode.

temperature in an electrolyte of 1.5 M KOH, 1.5 M KNO_3, or 0.5 M H_2SO_4, which have identical ion strengths. Before commencing any measurements, each carbon electrode was ultrasonically treated in the electrolyte solution to ensure the complete wetting of carbon micropores.

An impedance spectrum analyzer (IM6e, ZAHNER, Germany) equipped with the Thales software was employed to measure and analyze the ac impedance spectra. In the present work, the measurements were performed by applying a sinusoidal potential perturbation of small amplitude (5 mV), superimposed on a fixed dc potential varying within an appropriate potential window.

Results and Discussion

Figure 1 shows the cyclic voltammograms of the carbon/stainless steel electrode in the three electrolytes with a potential scan rate of 1 mV s^{-1}. The stainless steel was tested to be stable over the potential window applied for each electrolyte, giving no signal of water decomposition. The difference in potential window is expected because the redox potential of H_2O over an electrode is affected by the solution pH value. As a matter of fact, the open circuit potentials of the electrode are −0.25, −0.087, and +0.21 V versus Ag/AgCl for the KOH, KNO_3, and H_2SO_4 solutions, respectively. The voltammograms are not of a rectangular shape that is representative of the double layer formation mechanism. In the case of the KOH electrolyte, for example, the current value is larger at more negative potentials, indicating that the capacitance increases with the negative shift of the potential. This behavior was generally reported when KOH was used as the electrolyte.[23,24]

The performance of the composite electrode in KOH was analyzed by ac impedance spectroscopy, which distinguishes the resistance and capacitance of an electrode. The spectra obtained at different applied potentials are shown in Figure 2 as the standard Nyquist plot. For each spectrum, there is a semicircle intersecting the real axis in the high frequency region, and the plot transforms to a vertical line with decreasing frequency. This specific feature of impedance spectra has been generally reported for the carbon-based electrode systems.[10,11,24,25] The vertical line at low frequencies corresponds to the capacitive response of the porous carbons, and the data are generally employed to calculate the double layer capacitance, which is the major concern of a capacitor. The semicircle at high frequencies has been attributed to the existence of an interface, between the carbon and foil. The detailed mechanism causing this impedance response is rarely discussed, especially for the effects of the variation in the applied potential.

In general, the semicircle in the high frequency region is characteristic of a RC loop involving a capacitance in parallel with a resistance that is equivalent to the diameter of the semicircle.[10,25] If the semicircle is simply attributed to the contact of the carbon and foil, the variation of resistance with the applied potential, as observed in Figure 2, is not expected. The impedance response is more like that of a semiconducting material.[26] With the development of a depletion space charge region near the interface of a semiconductor at certain potentials, there is the presence of space charge capacitance and resistance in parallel, giving rise to a semicircle in the impedance spectra. The characteristics of the space charge region are strongly dependent on the applied potential.

As a matter of fact, a passive layer of iron or chromium oxides, which are of intrinsic semiconductors, is generally present on the surface of stainless steel.[14,15] The variation in the impedance behavior with the potential thus indicates that the performance of the carbon/foil composite electrode at high frequencies is, in fact, dominated by the semiconducting oxide film. To discuss the electrochemical behavior of the composite electrode, an equivalent circuit is proposed and shown in Figure 3a, in which a solution resistance, R_s, is in series with a RC loop, followed by a pure double layer capacitance responsible for the low frequency vertical lines in the Nyquist plot. The RC loop, consisting of a capacitance, C_b, and a resistance, R_b, in parallel, characterizes a space charge region. This model postulates that the region just inside the stainless steel foil interface has properties similar to those of semiconducting

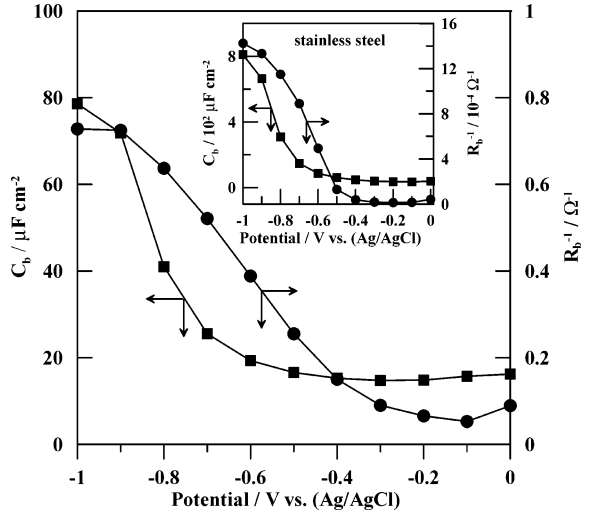

Figure 4. Variation of C_b and R_b in the space charge region with the applied potential in 1.5 M KOH for the carbon/stainless steel electrode. The inset shows the data for the stainless steel.

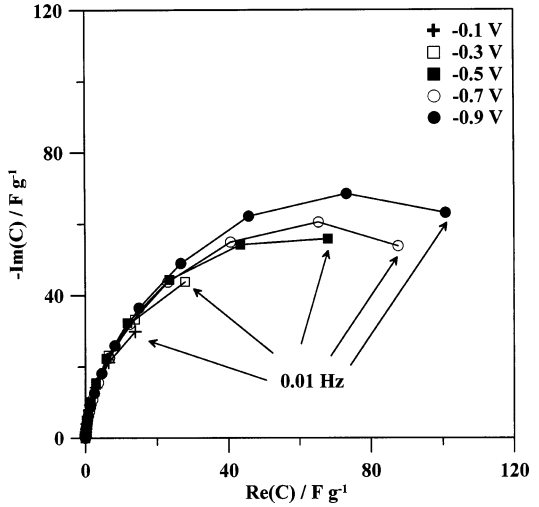

Figure 5. Complex plane plots of capacitance for the carbon/stainless steel electrode in 1.5 M KOH.

materials. The double layer capacitance of the electrolyte at the foil surface is large and can be neglected in the model. The contact resistance between carbon and foil is included in the measured R_b, though its contribution to R_b is relatively minor, especially under a depletion condition. The impedance, Z, of this equivalent circuit at high frequencies is given by

$$Z = R_s + \frac{R_b}{j\omega R_b C_b + 1} \tag{1}$$

where ω is the angular frequency and j the imaginary unit. The above equation corresponds to a locus showing a semicircle that intercepts the $Re(Z)$ axis at R_s and $R_s + R_b$ in the Nyquist plot. The data at high frequencies in Figure 2 are fitted to the equivalent circuit. The resulting values of the circuit element are summarized in Figure 4 except that of R_s, which is ~1.1 Ω irrespective of the applied potential.

Figure 4 shows that C_b decreases with a positive shift of the potential, while R_b increases (i.e., R_b^{-1} decreases). This response is similar to the electrochemical response of n-type semiconducting materials that own a potential-dependent space charge region. The decrease of C_b and R_b^{-1} can simply be attributed to a positive deviation from the flatband potential of the semiconducting oxide layer. The properties of the space charge region indeed affect the capacitive performance at low frequencies. This will be discussed.

To have a better perspective on the capacitive response, a plot of capacitance in the complex plane is given in Figure 5. Such capacitance is given by[27]

$$C = \frac{1}{j\omega Z} = \frac{1}{j\omega[Re(Z) + j\mathrm{Im}(Z)]} \tag{2}$$

This form of presentation is advantageous in visualizing the capacitive charging process in the low frequency region. The data in the capacitance complex plane are obtained by incorporation of eq 2 with low frequency impedance data in Figure 2. Incomplete semicircles can be observed in the complex plane. From extrapolation, the value at which the semicircles intersect the real axis represents the ultimate capacitance of the electrodes. The capacitance is seen to decrease with the positive shift of the potential, in agreement with the results of the cyclic voltammogram in Figure 1. In addition to the capacitance value, Figure 5 also shows that the completeness of the semicircle at 0.01 Hz reaches a higher degree at more negative potentials. This indicates that a faster capacitive response can be obtained at a more negative potential.

TABLE 1: Components and Related Parameters of the Serial RC Circuit (Figure 3b) for the Carbon/Stainless Steel Electrode at Different Potentials in 1.5 M KOH

potential (V)	C_d (F g^{-1})	R_{es} (Ω)	R_p (Ω)	τ_0 (s)
−1.0	143	3.1	1.7	8.0
−0.9	139	3.5	2.1	8.7
−0.8	132	3.7	2.1	8.8
−0.7	121	3.8	1.9	8.3
−0.6	117	4.7	2.1	9.9
−0.5	113	6.0	2.1	12.2
−0.4	106	8.7	2.0	16.6
−0.3	94	13.9	2.8	23.5
−0.2	85	19.8	4.6	30.3
−0.1	79	22.9	3.9	32.6

The overall resistance and capacitance of the electrodes based on an equivalent serial RC circuit (Figure 3b) can be estimated using the data in Figure 5, and the results are listed in Table 1. The double layer capacitance, C_d, is considered to be analogous to that determined from constant-current discharge. The resistance thus determined is the so-called equivalent series resistance, R_{es}, which is composed of the electrolyte resistance, R_s, electrode resistance, R_b, and electrolyte resistance in pores, R_p.[28] The values of R_p are calculated by subtracting R_s and R_b from R_{es} and shown in Table 1 as well. It is found that the resistance in pores has a minor contribution to the overall resistance, R_{es}, especially at more positive potentials. The electrode resistance, R_b, has a significant contribution to the overall resistance, and this renders that the R_{es} value, as well as the serial RC time constant, τ_0 ($=R_{es} \times C_d$), determined from the low frequency data, is smaller at a more negative potential. It has to be noted that R_b is the space charge resistance determined from the high frequency data (i.e., the semicircle in Figure 2), while the time constant, τ_0, is considered to be a characteristic constant of the capacitive behavior exhibited in the low frequency region (i.e., τ_0 is the reciprocal of the frequency at which the maximum $-\mathrm{Im}(C)$ occurs on the semicircle in Figure 5).[27] This is an indication that the performances of this capacitor system at high and low frequencies are closely related.

Comparing the data in Table 1 and Figure 4 shows that the double layer capacitance of the carbon is a decreasing function of R_b. This reflects that energy dissipation of this electron-transfer process occurs mainly at the passive layer, the resistance

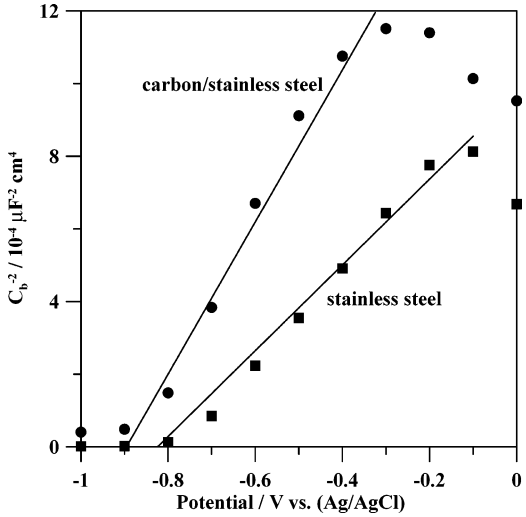

Figure 6. Variation of C_b with the applied potential in 1.5 M KOH presented in the Mott−Schottky relationship for the carbon/stainless steel electrode and the stainless steel foil.

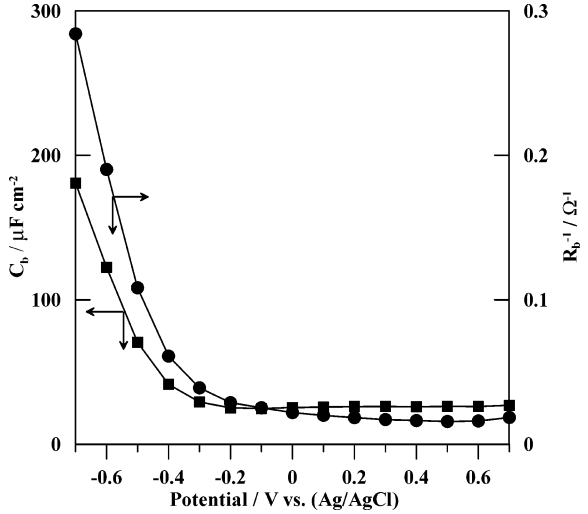

Figure 7. Variation of C_b and R_b in the space charge region with the applied potential in 1.5 M KNO_3.

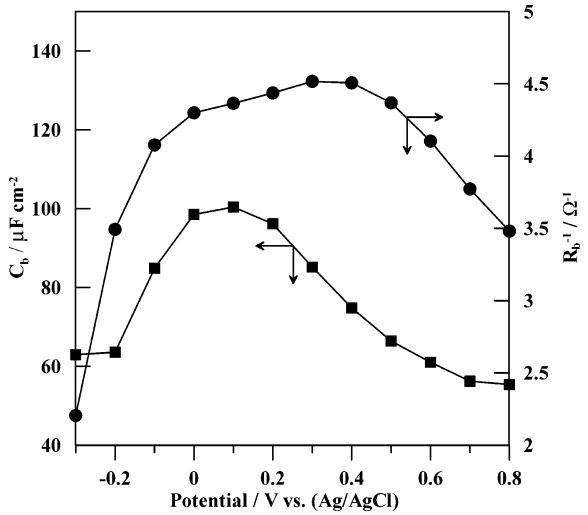

Figure 8. Variation of C_b and R_b in the space charge region with the applied potential in 0.5 M H_2SO_4.

of which is potential dependent. Thus, the influence of the potential window applied, as well as the type of electrolyte employed, on the semiconductor layer should be taken into account in optimizing the operation of this energy-storage process. Because of the great influence of the oxide layer on the capacitive performance, the high frequency data were subjected to analysis using the Mott−Schottky equation,[29−33] which correlates the space charge capacitance and the applied potential across a depletion space charge layer, that is,

$$\frac{1}{C^2} = \left(\frac{2}{e\epsilon\epsilon_0 N_D}\right)\left(V - V_{FB} - \frac{kT}{e}\right) \qquad (3)$$

where ϵ_0 represents the vacuum permittivity, ϵ the dielectric constant of the passive oxide layer, e the electron charge, V the applied potential, V_{FB} the flatband potential, k the Boltzmann constant, T the absolute temperature, and N_D the donor density. The temperature term is generally small and can be neglected. According to the Mott−Schottky equation, a linear relationship of C^{-2} versus V can be observed. The data in Figure 4 are transformed into a relation of C^{-2} versus V in Figure 6. A linear relationship can be observed within −0.4 and −0.9 V, in agreement with previous studies that reported the Mott−Schottky behavior of stainless steel foils in a basic solution.[14,15] Extrapolation of the linear relationship to a C^{-2} value of zero gives the value of V_{FB}. Figure 6 shows a V_{FB} value of ∼ −0.9 V. The positive value of the slope reflects the n-type semiconductor behavior of the passive layer.

The impedance responses of the composite electrode in neutral and acidic electrolytes were also analyzed. In the case of neutral KNO_3, the values of C_b and R_b^{-1} (Figure 7) show a sharp decrease around −0.5 V and a leveling-off at more positive potentials. According to the preceding interpretation, this impedance response correlates well with the cyclic voltammogram in Figure 1, which shows a current decrease with a positive shift of the potential near −0.5 V and a leveling-off at more positive potentials. The data in Figure 7 were fitted to the Mott−Schottky equation, and a flatband potential of ∼ −0.55 V for a n-type semiconductor was obtained. The variation of the flatband potential with pH value is expected and has been extensively discussed.[34,35] With further increase of the electrolyte acidity by using H_2SO_4, the trend of C_b and R_b^{-1} variations with the applied potential becomes sophisticated, as depicted in Figure 8. The values of C_b and R_b^{-1} increase with the positive potential shift to reach a maximum near 0.2−0.4 V, then followed by a decrease with further positive shift of the potential. Similar to the cases in KOH and KNO_3, the variation of C_b and R_b^{-1} is in good agreement with the voltammogram in Figure 1, showing a vague peak current around 0.2−0.4 V.

The Mott−Schottky relationship in H_2SO_4 is shown in Figure 9. A p-type semiconductor behavior is observed in the more negative potential region and a n-type behavior in the more positive region. The linear extrapolation of the two regions has an intersection near their flatband potentials, which are of ∼0.1 V for both types of semiconductors. The maximum double layer capacitance would occur in the neighborhood of the flatband potentials, at which the lowest overall R_b, contributed by the two types of semiconductors, can be observed. Deviation of the potential from the flatband position would result in the formation of a depletion layer to increase R_b and thus the suppression of the double layer capacitance. The space charge resistance is much smaller in H_2SO_4 than in the other electrolytes, as indicated by the larger value of R_b^{-1}. This can be ascribed to the fact that the potentials applied in H_2SO_4 are relatively close to the flatband potentials of the two semicon-

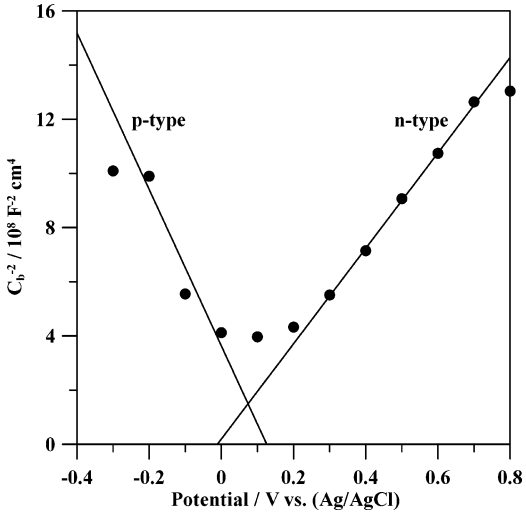

Figure 9. Variation of C_b with the applied potential in 0.5 M H_2SO_4 presented in the Mott−Schottky relationship.

ductors. There is a corresponding larger capacitance for H_2SO_4 observed from the voltammograms in Figure 1.

The transition of the semiconducting behavior in H_2SO_4 can be attributed to the fact that the passive layer contains both iron and chromium oxides, which are intrinsic semiconductors of the n and p types, respectively.[14,15] At more negative potentials, the n-type semiconductor behaves like a metallic species because its space charge region is situated under an accumulation condition. Thus, the semiconducting behavior is dominated by that of the p-type semiconductor at more negative potentials, and vice versa at more positive potentials. As to the cases using KOH and KNO_3 as electrolyte, there is no maximum value of C_b or R_b^{-1} observed. This suggested that in basic or neutral electrolytes the flatband potential of the p-type semiconductor is more negative than that of the n-type one; that is, there is no intersection of the linear Mott−Schottky lines, as shown in Figure 9. Under this circumstance, the p-type semiconductor only forms an accumulation space charge region throughout the potential range applied and the impedance measurements showed only n-type semiconducting behavior.

To confirm that the high frequency impedance behavior of the composite electrode is dominated by the passive oxide layer of the stainless steel foil, auxiliary impedance experiments were conducted to analyze the foil in different electrolytes. The equivalent circuit in Figure 3a was employed to determine R_b and C_b at the foil/solution interface, except that the pure double layer capacitance element was omitted. The impedance data for the stainless steel foil in NaOH are given in Figures 2, 4, and 6. Very large values of R_b were obtained, as reflected in Figures 2 and 4, because little charge transfer occurs across the interface. The variation of C_b with the applied potential was analyzed with the Mott−Schottky equation. Figure 6 shows that the flatband potential obtained for the foil was similar to that for the composite electrode. This finding supports the argument that the electrochemical behavior of the carbon/foil interface is governed by the semiconducting properties of the passive layer.

Summary and Conclusions

The present work has demonstrated that the semiconducting passive oxide layer of the stainless steel current collector significantly affects the capacitive performance of porous carbon equipped in an electric double layer capacitor. Impedance analysis reflected that the electrochemical behavior of the carbon/stainless steel composite electrode in the high frequency region is dominated by the space charge region of the passive layer. The space charge resistance has the major contribution to the overall resistance of the composite electrode, especially for applied potentials deviating from the flatband to form a depletion layer. The double layer capacitance of the carbon, measured from cyclic voltammetry or low frequency impedance, was found to be a decreasing function of the space charge resistance of the passive layer. This reflects that a significant amount of energy dissipation occurs at the passive layer in the energy-storage process.

The electrochemical behavior of the passive layer is affected by the electrolyte employed. In the potential range used for the H_2SO_4 electrolyte, both the n- and p-type semiconducting behaviors in the depletion situation can be detected. For the KNO_3 and KOH electrolytes, the depletion behavior was detected only for the n-type oxide, while the p-type one was situated under the accumulation condition in the potential range employed. Because the potentials applied in H_2SO_4 were in the neighborhood of the flatband potentials, the double layer capacitance of the carbon in H_2SO_4 is larger than those in the other two electrolytes due to the smaller space charge resistance present in the passive layer.

Acknowledgment. Financial support from the National Science Council of Taiwan (NSC93-2214-E−006-005), the Center for Micro/Nano Technology Research, National Cheng Kung University, under projects from the Ministry of Education and the National Science Council (NSC 93-212−M-006-006) of Taiwan, and NCU-ITRI Joint Research Project of National Central University (NCU-ITRI 930202) is gratefully acknowledged.

References and Notes

(1) Kötz, R.; Carlen, M. *Electrochim. Acta* **2000**, *45*, 2483.
(2) Kinoshita K. *Carbon: Electrochemical and Physicochemical Properties*; John Wiley and Sons: New York, 1988.
(3) Tanahashi, I.; Yoshida, A.; Nishino, A. *Carbon* **1990**, *28*, 477.
(4) Biniak, S.; Dzieleńdziak, B.; Siedlewski, J. *Carbon* **1995**, *33*, 1255.
(5) Liu, X.; Osaka, T. *J. Electrochem. Soc.* **1997**, *144*, 3066.
(6) Qu, D.; Shi, H. *J. Power Sources* **1998**, *74*, 99.
(7) Weng, T.-C.; Teng, H. *J. Electrochem. Soc.* **2000**, *148*, A368.
(8) Frackowiak, E.; Béguin, F. *Carbon* **2001**, *39*, 937.
(9) Hsieh, C.-T.; Teng, H. *Carbon* **2002**, *40*, 667.
(10) Nian, Y.-R.; Teng, H. *J. Electrochem. Soc.* **2002**, *149*, A1008.
(11) Nian, Y.-R.; Teng, H. *J. Electroanal. Chem.* **2003**, *540*, 119.
(12) Lozano-Castelló, D.; Cazorla-Amorós, D.; Linares-Solano, A.; Shiraishi, S.; Kurihara, H.; Oya, A. *Carbon* **2003**, *41*, 1765.
(13) Soneda, Y.; Toyoda, M.; Hashiya, K.; Yamashita, J.; Kodama, M.; Hatori, H.; Inagaki, M. *Carbon* **2003**, *41*, 2680.
(14) Hakiki, N. E.; Boudin, S.; Rondot, B.; Belo, M. D. C. *Corros. Sci.* **1995**, *37* (11), 1809.
(15) Belo, M. D. C.; Rondot, B.; Compere, C.; Montemor, M. F.; Simões, A. M. P.; Ferreira, M. G. S. *Corros. Sci.* **1998**, *40*, 481.
(16) Bisquert, J.; Garcia-Belmonte, G.; Fabregat-Santiage, F.; Ferriols, N. S.; Bogdanoff, P.; Pereira, E. C. *J. Phys. Chem. B* **2000**, *104*, 2287.
(17) Fabregat-Santiage, F.; Garcia-Belmonte, G.; Bisquert, J.; Zaban, A.; Salvador, P. *J. Phys. Chem. B* **2002**, *106*, 334.
(18) Fabregat-Santiage, F.; Mora-Seró, I.; Garcia-Belmonte, G.; Bisquert, J. *J. Phys. Chem. B* **2003**, *107*, 758.
(19) Macdonald, J. R. *Bull. Am. Phys. Soc.* **1985**, *30*, 587.
(20) Macdonald, J. R.; Johnson, W. B. *Impedance Spectroscopy: Emphasizing Solid Materials and Systems*; Macdonald, J. R., Ed.; John Wiley and Sons: New York, 1987.
(21) Bard, A. J.; Faulkner, L. R. *Electrochemical Methods, Fundamentals and Applications*, 2nd ed.; John Wiley and Sons: New York, 2001.
(22) Conway, B. E. *Electrochemical Supercapacitors*; Kluwer Academic/Plenum: New York, 1999.
(23) Frackowiak, E.; Béguin, F. *Carbon* **2001**, *39*, 937.
(24) Deyang, Q. *J. Power Sources* **2002**, *109*, 403.
(25) Momma, T.; Liu, X.; Osaka, T.; Ushio, Y.; Sawada, Y. *J. Power Sources* **1996**, *60*, 249.
(26) Chemla, M.; Bertagna, V.; Erre, R.; Rouelle, F.; Petitdidier, S.; Levy, D. *Electrochem. Solid-State Lett.* **2003**, *6*, G7.

(27) Taberna, P. L., Simon, P., Fauvarque, J. F. *J. Electrochem. Soc*. **2003**, *150*, A292.
(28) Yoon, S.; Lee, J.; Hyeon, T.; Oh, S. M. *J. Electrochem. Soc*. **2000**, *147*, 2507.
(29) Abshere, T. A.; Richmond, G. L. *J. Phys. Chem. B* **2000**, *104*, 1602.
(30) Hens, Z.; Gomes, W. P. *J. Phys. Chem. B* **2000**, *104*, 7725.
(31) Yu, H. Z.; Morin, S.; Wayner, D. D. M. *J. Phys. Chem. B* **2000**, *104*, 11157.
(32) Raisch, P.; Haiss, W.; Nichols, R. J.; Schiffrin, D. J. *J. Phys. Chem. B* **2001**, *105*, 12508.
(33) Watson, D. F.; Marton, A.; Stux, A. M.; Meyer, G. J. *J. Phys. Chem. B* **2003**, *107*, 10971.
(34) Sato, N. *Electrochemistry at Metal and Semiconductor Electrodes*; Elsevier: Amsterdam, The Netherlands, 1998.
(35) Memming, R. *Semiconductor Electrochemistry*; Wiley-VCH: Weinheim, Germany, 2001.